Inherent Impedance Transformation and Isolation in Dual-Band Balun For RF Front End Applications

Rahul Gupta, *Young IEEE Member*, Andrey A.Yelizarov, *Senior IEEE Member*, Igor V.Nazarov, Elmira A.Zakirova, Alexandr D.Kasatkin

Electronic Engineering Department
HSE University
rgupta@hse.ru, a.yelizarov@hse.ru, inazarov@hse.ru, ezakirova@hse.ru, adkasatkin@hse.ru

***Abstract*— This paper presents a balun architecture with the inherent impedance transformation between the balanced and unbalanced ports. Also, the balun provides the isolation between the balanced ports while working at the two arbitrary frequencies concurrently. The systematic design analysis with the closed-form design equations is provided in the paper to design the prototype of the proposed balun architecture. The working of the proposed balun architecture is also demonstrated through the electromagnetic simulation on an industry standard simulation tool working at a frequency ratio (r =2) and impedance ratio (k=2). The simulation results are in good agreement with the calculated results.**

Keywords—balun; dual-band; impedance transformation; isolation; microstrip transmission line; equivalent circuit analysis

I. INTRODUCTION

A Balun is an indispensable element in the RF front end of a telecommunication system. The key application areas of a balun include mixers, antenna feeding networks, power amplifiers, etc. [1]-[2]. The main functionality of a balun is to transform the unbalanced signals (single-ended) to the balanced signals (differential-ended) and vice-versa without altering the key signal properties. Also, the balun is used to transform the impedances between the balanced and unbalanced ports [3]-[5].

A simplified architecture of balun is presented in [6] to demonstrate its operation. There are numerous reports on the dual-band baluns working concurrently at two arbitrary frequencies [5], [7]–[15]. Also, the design includes the impedance transformation capability in the design of baluns inherently [12]–[15] have reported the inherent impedance transformation. A recent dual-band balun [12] with demonstrated impedance transformation capability, however, may struggle with the layout complexity for its longer transmission line associated with the T-junction coupled line.

To advance the dual-band balun technology, this paper, therefore, reports high inherent impedance transforming dual-band balun working at arbitrarily separated two design frequencies. The proposed design is capable of working at arbitrary frequency ratios and impedance transformation ratios while maintaining the performance matrices of a balun. The symmetry of the proposed architecture enables analysis using odd-even mode analysis and this helps in deducing the closed-form design equations. Some design cases are provided to demonstrate the balun's capability at extreme specifications.

In this work, a novel architecture of the balun is presented with inherent impedance transformation at the two arbitrary design frequencies. In addition, following the balun properties, all the ports are matched, the balanced ports are isolated from each other, and the phase difference between the output ports is 180°. Since in a three ports lossless device, simultaneous all port matching and isolation cannot be provided [16], therefore, a lumped resistor is used to compensate for the lossless architecture. The analytical solution of the proposed architecture is also provided with closed-form design equations. All the performance matrices are also validated through electromagnetic simulation (EM) on an industry-standard simulation tool and provided in this paper.

II. PROPOSED ARCHITECTURE

The basic architecture of the proposed dual-band balun, shown in Fig 1, is a three-port device, utilizing two edge coupled-lines in the structure of the balun as the core. The circuit is symmetric around Y-Axis and hence can be analyzed using the even-odd mode technique. The respective even- and odd-mode equivalent circuits are given in Figs. 2 and 3 respectively. It must be noted that these equivalent circuits must satisfy (1) and (2) for successful balun operation. In (1) and (2), the term *Zodd* is the odd-mode impedance at the input port and *Teven* is the transmission of signal in the even-mode.

$$Z_{odd} = 2Z_s \quad (1)$$

$$T_{even} = 0 \quad (2)$$

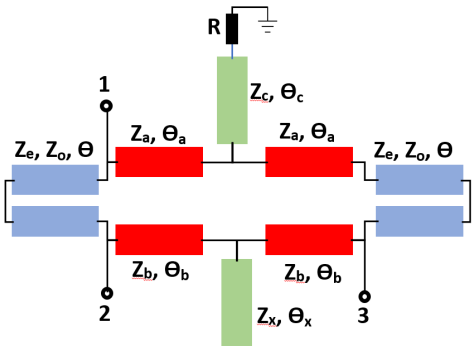

Fig. 1. Proposed 3-Ports balun architecture.

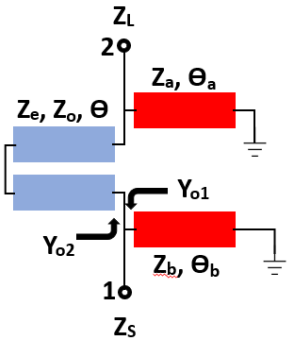

Fig. 2. Odd mode equivalent circuit of the proposed balun.

A. *Odd-mode Equivalent Circuit Analysis*

The odd mode equivalent circuit, in Fig. 2, results when the junctions along the symmetric Y-Axis are shorted to the ground. In such a situation, the transmission line with electrical lengths θ_1 and θ_2 is shorted to ground. The terms Y_{o1} and Y_{o2} marked in Fig. 2 are respective admittances and can be obtained from usual circuit analysis. Looking from port 1, the load admittance for the coupled line (Z_e, Z_o, θ) will be the parallel combination of the admittances offered by port 2 and short-circuited stub (Z_a, θ_a). Further, to follow (1), the real part of the admittance Y_{o2} can be equated with the equivalent source admittance as given in (3).

$$Re\{Y_{o2}\} = \frac{1}{2Z_S} \tag{3}$$

Solving (3) yields the expression of Z_a in form of Z_e, Z_o, θ, θ_a, and Z_L, as depicted in (4). For the simplicity, the electrical lengths of the architecture are assumed equal here, i.e., $\theta = \theta_a$.

$$Z_a = \frac{2Z_L Z_e Z_o (A)}{B} \tag{4}$$

Where,

$$A = \sqrt{2}\sqrt{Z_S Z_L Z_o^2 - \frac{2Z_e^2 Z_o^2}{\tan^2\theta} + \frac{Z_S Z_L Z_o^2}{\tan^4\theta} + \frac{2Z_S Z_L Z_o Z_o}{\tan^2\theta}} \pm \left(\frac{Z_L Z_o}{\tan^2\theta} - Z_L Z_o\right) \tag{4}$$

$$B = -\frac{Z_L^2 Z_e^2}{\tan^2\theta} + 2Z_L^2 Z_e Z_o - Z_L^2 Z_o^2 \tan^2\theta + \frac{2Z_S Z_L Z_e^2}{\tan^2\theta} + 4Z_S Z_L Z_e Z_o + 2Z_S Z_L Z_o^2 \tan^2\theta - 4Z_e^2 Z_o^2 \tag{5}$$

Furthermore, the electrical length θ follows (6) for the dual-band operation. Here, f_1 and f_2 are the lower and upper frequencies of operation, respectively. And r is the frequency ratio, i.e., $r = f_2/f_1 \geq 1$ and n ∈ I.

$$\theta = \frac{(1+n)\pi}{1+r} \tag{6}$$

Also, the parameters Z_e and Z_o are considered as independent variables and can be chosen in the realizable limit of the microstrip technology [20 160] Ω in order to get the realizable value of Z_a again within the microstrip technology. Please also note that Z_e and Z_o are correlated with other for a desired coupling factor (ρ), i.e., $\rho = Z_e / Z_o$.

The imaginary part of Y_{o2} should be cancelled with the equivalent admittance offered by the short-circuited stub (Z_b, θ_b) which shall result in the expression of Z_b as expressed in (7).

$$Z_b = \frac{C+D}{E+F} \tag{7}$$

$$C = \frac{(2Z_a Z_o + Z_a Z_a - Z_o Z_a \tan^2\theta)^2}{Z_a^2 (Z_o \tan^2\theta + Z_a)^2} \tag{8}$$

$$D = 4Z_e^2 Z_o^2 \tan^2\theta \,/\, Z_L^2 (Z_o \tan^2\theta + Z_e)^2 \tag{9}$$

$$E = (Z_o \tan^2\theta - Z_e + 2Z_a \tan^2\theta) * \frac{(2Z_a Z_o + Z_a Z_a - Z_o Z_a \tan^2\theta)}{Z_a^2 (Z_o \tan^2\theta + Z_a)^2} \tag{10}$$

$$F = \frac{2Z_a Z_o \tan^2\theta (Z_a - Z_o \tan^2\theta)}{Z_L^2 (Z_o \tan^2\theta + Z_a)^2} \tag{11}$$

B. *Even-mode Equivalent Circuit*

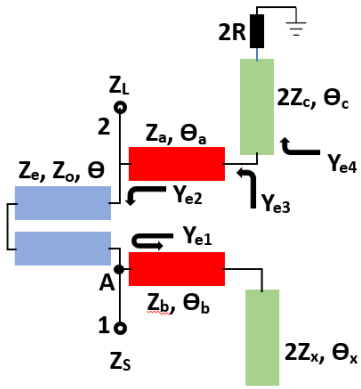

Fig. 3. Even mode equivalent circuit of the proposed balun.

The even mode equivalent circuit, in Fig. 3, results when the junctions along the symmetric Y-Axis are turned to open circuit condition. In such a situation, the characteristics impedance of the transmission lines along the Y-Axis is doubled, i.e., $2Z_a$ and $2Z_X$ respectively for the two transmission lines (Z_c, θ_c) and (Z_X, θ_X). The terms Y_{e1}, Y_{e2}, Y_{e3}, and, Y_{e4}, marked in Fig. 3, are respective admittances and can be obtained from usual circuit analysis.

For successful balun operation, the transmission in even-mode must be zero, i.e. signal must not flow from port 1 (input port) to port 2 and port 3 (output ports), as identified by (2). This is achieved by creating a virtual ground at the node A in Fig. 3 and is expressed by (12). This will then effectively lead to the expression of Z_x in (13).

$$Y_{e1} = \infty \tag{12}$$

Again, for $\theta_b = \theta_x = \theta$;

$$Z_X = \frac{1}{2}(Z_b \tan^2\theta) \quad (13)$$

Now in order to provide the isolation between the output ports the all ports matching must be ensured in the even mode analysis [6]. This can be maintained by following eq. (14).

$$Y_{e3} = Y_{e4}^* \quad (14)$$

Solving this equation yields the expressions of Z_c and R as provided in (15) and (16).

$$Z_c = -[2B_{e2}Z_a^2 + Z_a^2 \sin 4\theta - Z_a\sqrt{2(G\cos 4\theta + H\sin 4\theta + I)} + 2B_{e2}Z_a^2\cos 4\theta - B_{e2}^2 Z_a \cos 4\theta]/[4\sin 2\theta\,(B_{e2}^2 + G_{e2}^2 + Z_a^2) - 4B_{e2}Z_a + 2\sin 4\theta\,(Z_a^2 - B_{e2}^2 - G_{e2}^2) + 4B_{e2}Z_a\cos 4\theta] \quad (15)$$

$$R = Z_c\sqrt{\frac{J}{K(\tan\theta)}} \quad (16)$$

Where,

$$G = -G_{e2}^4 - Z_a^4 - B_{e2}^4 + 6B_{e2}^2Z_a^2 - 2G_{e2}^2Z_a^2 - 2B_{e2}^2G_{e2}^2 \quad (17)$$

$$H = 4B_{e2}Z_a^3 - 4B_{e2}^3Z_a - 4B_{e2}G_{e2}^2Z_a \quad (18)$$

$$I = B_{e2}^4 + G_{e2}^4 + 2B_{e2}^2G_{e2}^2 + Z_a^4 + 2B_{e2}^2Z_a^2 + 2G_{e2}^2Z_a^2 \quad (19)$$

$$J = -B_{e2}^2Z_a + 2Z_cB_{e2}^2\tan^2\theta - B_{e2}Z_a^2\tan\theta + \frac{B_{e2}Z_a^2}{\tan\theta} + Z_a^3 - 4Z_cB_{e2}Z_a\tan\theta - G_{e2}^2Z_a + 2Z_cG_{e2}^2\tan^2\theta + 2Z_cZ_a^2 \quad (20)$$

$$K = B_{e2}^2Z_a\tan\theta + 2Z_cB_{e2}^2\tan\theta + B_{e2}Z_a^2\tan^2\theta - B_{e2}Z_a^2 - 4Z_cZ_aB_{e2} + Z_aG_{e2}^2\tan\theta + 2Z_cG_{e2}^2\tan\theta - Z_a^3\tan\theta + \frac{2Z_cZ_a^2}{\tan\theta} \quad (21)$$

And,

$$G_{e2} = \frac{4Z_L^2Z_c^2Z_0^2\tan^2\theta}{Z_L^2(Z_c - Z_0\tan^2\theta)^2 + 4Z_c^2Z_0^2\tan^2\theta} \quad (22)$$

$$B_{e2} = \frac{2Z_L^2Z_cZ_0\tan\theta(Z_c - Z_0\tan^2\theta)}{Z_L^2(Z_c - Z_0\tan^2\theta)^2 + 4Z_c^2Z_0^2\tan^2\theta} \quad (23)$$

Please note that for the ease of deducing the expressions, all the electrical lengths are assumed equal, i.e., $\theta = \theta_a = \theta_b = \theta_c = \theta_X$.

III. Design Procedure for the Proposed Balun

The proposed architecture and the derived expressions are verified through a design of balun with the defined specifications. It is assumed to validate the performance at the frequency and impedance ratios of 2, i.e., the lower frequency 1 GHZ and the upper frequency 2 GHz and the source impedance 50 Ω and load impedances 100 Ω. For the assumed specifications, the proposed design theory is utilized to calculate the design parameters of the proposed balun. Following the simple steps mentioned below, the design parameters of the proposed balun can be calculated for any given specifications:

- Using (4), Z_a is calculated to be 72.9 Ω.
- Here, for the dual-band operation, the electrical length Θ is calculated as 60˚ using (6). And the even- and odd-mode impedances of the coupled line are assumed as Z_e = 125 Ω and Z_o = 65 Ω.
- Further, Z_b is calculated to be 74 Ω using (7).
- Usign Z_b, Z_X can be calculated from (13) as 111 Ω.
- Now, Zc and R are calculated as 23.6 Ω and 20 Ω using (15) and (16) respectively.

IV. EM Simulation Results

The working of the designed balun in the previous section is also verified through electromagnetic simulation (EM) using an industry-standard electronic design and automation (EDA) tool. The EM simulation of the balun is performed with the Rogers substrate RO4003 with dielectric permittivity 3.38 and the loss tangent 0.0027. The thickness of the substrate is 1.52 mm and the copper thickness on both sides of the laminates is 35 µm. The balun is further optimized for all the bends and discontinuities in the design and the overall dimensions of the proposed balun for the designed specifications are 123.8 mm and 33.7 mm. The EM layout is also depicted in Fig. 4.

The EM simulation results are also plotted in Figs. 5, 6, and 7. The matching at all the ports (S11, S22, and S33) of the proposed balun is verified and depicted in Fig. 5. The values of the obtained matching are mentioned in Table 1. The isolation between the output ports (S23) is plotted in Fig. 6 along with the insertion losses at ports 2 and 3 (S21 and S31). The values of these obtained parameters are mentioned in Table 1. Finally, the phase difference between the output ports is also plotted in Fig. 7 with a comparison of the results obtained using the calculated results with ideal transmission lines. All the results are mentioned in Table 1 and are in good coordination with the calculated values and thus verifies the design procedure and methodology.

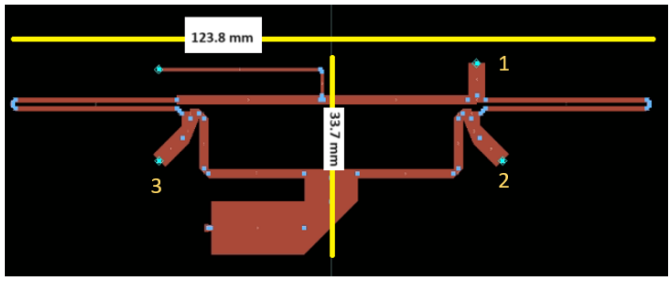

Fig. 4. The layout of the proposed balun for r=2 and k=2 (Port 1 on the top, Ports 2 and 3 on the bottom).

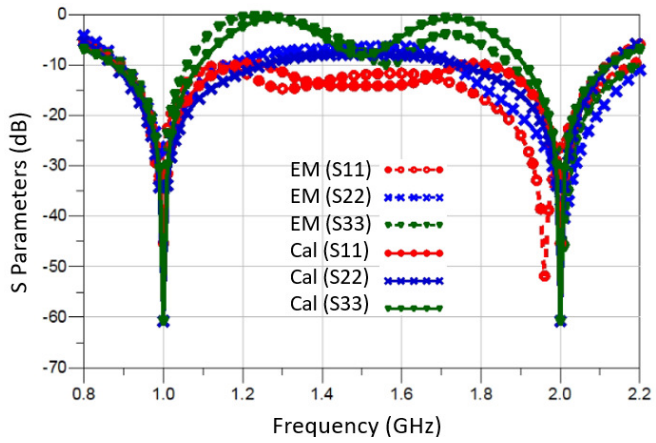

Fig. 5. All ports matching comparison results of the proposed balun (EM: electromagnetic simulation, Cal: Calculated)

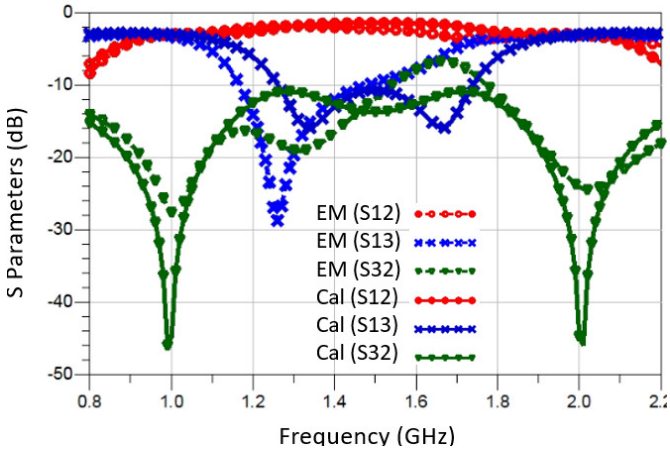

Fig. 6. Insertion loss and isolation between the output ports comparison results of the proposed balun (EM: electromagnetic simulation, Cal: Calculated)

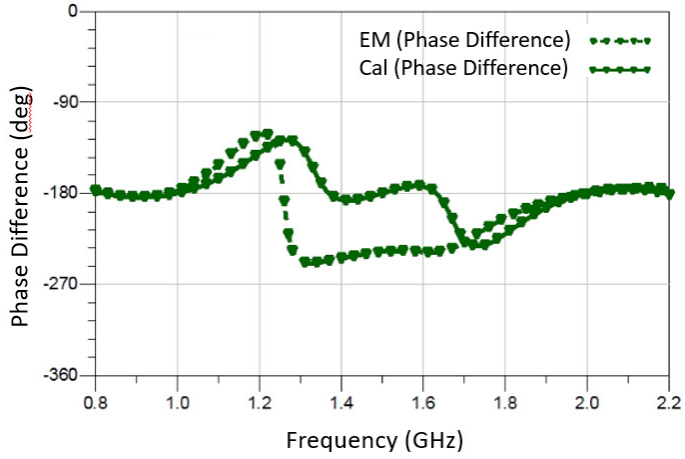

Fig. 7. Phase difference between the output ports (balanced) comparison results of the proposed balun (EM: electromagnetic simulation, Cal: Calculated)

Table 1. EM simulation results of the proposed balun

S_{11} (dB)		**S_{22} (dB)**		**S_{33} (dB)**	
1 GHz	**2 GHz**	**1 GHz**	**2 GHz**	**1 GHz**	**2 GHz**
-26.9	-26.4	-28.3	-36.8	-32.8	-32.5
S_{21} (dB)		**S_{31} (dB)**		**S_{32} (dB)**	
1 GHz	**2 GHz**	**1 GHz**	**2 GHz**	**1 GHz**	**2 GHz**
-3.0	-3.2	-3.3	-3.2	-27.6	-24.1
Phase Difference (°)					
1 GHz	**2 GHz**				
-178.0	-180.4				

V. Conclusion

A dual-frequency balun architecture with impedance transformation has been presented in this paper. The balun has also exhibited good isolation between the two output (balanced) ports. The design methodology has also introduced two independent design variables which has improved the design flexibility to provide the realizable design parameters for the required design specifications. The closed-form design equations with the design procedure have also been provided which enables prototyping of the design for different specifications. The EM simulation performance of the designed balun is also provided with which the agreement between the calculated results is apparent. Thus, the proposed design methodology has been validated.

VII. Acknowledgement

The publication was prepared within the framework of the Academic Fund Program at HSE University (grant №23-00-003 “Research of technologies and devices for wireless transfer of electromagnetic energy for high-speed mobile and wearable devices of the Internet of things (IoT / IIoT) and cyber-physical systems”).

References

[1] W. Feng, Y. Shi, X. Y. Zhou, X. Shen and W. Che, "A Bandpass Push–Pull High Power Amplifier Based on SIW Filtering Balun Power Divider," IEEE Transactions on Plasma Science, vol. 47, no. 9, pp. 4281-4286, Sept. 2019, doi: 10.1109/TPS.2019.2932083.

[2] H. Mohammadnezhad, H. Wang, and P. Heydari, “Analysis and design of a wideband, balun-based, differential power splitter at mm-wave,” *IEEE Trans. Circuits Syst. II, Exp. Briefs*, vol. 65, no. 11, pp. 1629–1633, 2018.

[3] G. R. Friedrichs, L. Boskovic and D. S. Filipovic, "Design of Dual-Polarized Log-Periodic Antenna with Embedded Balun Impedance Transformer," 2020 IEEE International Symposium on Antennas and Propagation and North American Radio Science Meeting, Montreal, QC, Canada, 2020, pp. 1379-1380, doi: 10.1109/IEEECONF35879.2020.9329975.

[4] C. Pakasiri and K. Nithiporndecha, "A 433 MHz compact complex impedance-transforming balun," 2017 International Symposium on

Antennas and Propagation (ISAP), Phuket, Thailand, 2017, pp. 1-2, doi: 10.1109/ISANP.2017.8229015.

[5] R. Gupta, S. Kairatova, M. Hashmi and G. Nauryzbayev, "A Dual-Band Balun Architecture With Unequal Port-Terminations," 2020 50th European Microwave Conference (EuMC), Utrecht, Netherlands, 2021, pp. 848-851, doi: 10.23919/EuMC48046.2021.9337973.

[6] R. Gupta, M. A. Maktoomi and M. S. Hashmi, "A new high frequency balun with simplified impedance matching technique," 2016 Asia-Pacific Microwave Conference (APMC), New Delhi, India, 2016, pp. 1-4, doi: 10.1109/APMC.2016.7931394.

[7] H. Zhang, Y. Peng, and H. Xin, "A tapped stepped-impedance balun with dual-band operations," *IEEE Antennas Wirel. Propag. Lett.*, vol. 7, pp. 119–122, 2008.

[8] F. Huang, J. Wang, L. Zhu, Q. Chen, and W. Wu, "Dual-band microstrip balun with flexible frequency ratio and high selectivity," *IEEE Microw. Wirel. Compon. Lett.*, vol. 27, no. 11, pp. 962–964, Nov 2017.

[9] J. Li, J. Li, J. Yin, C. Guo, H. Zhai and Z. Zhao, "A Miniaturized Dual-Band Dual-Polarized Base Station Antenna Loaded With Duplex Baluns," in IEEE Antennas and Wireless Propagation Letters, vol. 22, no. 7, pp. 1756-1760, July 2023, doi: 10.1109/LAWP.2023.3262824.

[10] L. K. Yeung and K. -L. Wu, "A Dual-Band Coupled-Line Balun Filter," in IEEE Transactions on Microwave Theory and Techniques, vol. 55, no. 11, pp. 2406-2411, Nov. 2007, doi: 10.1109/TMTT.2007.907402.

[11] H. Zhang and H. Xin, "A Dual-Band Dipole Antenna With Integrated-Balun," IEEE Transactions on Antennas and Propagation, vol. 57, no. 3, pp. 786-789, March 2009, doi: 10.1109/TAP.2009.2013440.

[12] R. Gupta, M. S. Hashmi and M. H. Maktoomi, "An Enhanced Frequency Ratio Dual Band Balun Augmented With High Impedance Transformation," IEEE Transactions on Circuits and Systems II: Express Briefs, vol. 67, no. 12, pp. 2973-2977, Dec. 2020, doi: 10.1109/TCSII.2020.2984787.

[13] W. Zhang, Z. Ning, Y. Wu, C. Yu, S. Li, and Y. Liu, "Dual-band out-of-phase power divider with impedance transformation and wide frequency ratio," *IEEE Microw. Wirel. Compon. Lett.*, vol. 25, no. 12, pp. 787–789, Dec 2015.

[14] Y. Wu, L. Yao, W. Zhang, W. Wang, and Y. Liu, "A planar dual-band coupled-line balun with impedance transformation and high isolation," *IEEE Access*, vol. 4, pp. 9689–9701, 2016.

[15] E. S. Li, C. Lin, H. Jin, and K. Chin, "A systematic design method for a dual-band balun with impedance transformation and high isolation," *IEEE Access*, vol. 7, pp. 143 805–143 813, 2019.

[16] R. Gupta and M. Hashmi, "High impedance transforming simplified balun architecture in microstrip technology," *Microw. Opt. Technol. Lett.*, vol. 60, no. 12, pp. 3019–3023, Dec. 2018.